Journal of
Ceramic Science
and Technology

J. Ceram. Sci. Tech., **05** [04] 275-280 (2014)
DOI: 10.4416/JCST2014-00025
available online at: http://www.ceramic-science.com

Preparation of Ceramic Nanoparticles by CO_2 Laser Vaporization

H.-D. Kurland, J. Grabow, Chr. Stötzel, F.A. Müller*

Otto-Schott-Institute of Materials Research (OSIM), Friedrich Schiller University Jena, Löbdergraben 32, 07743 Jena, Germany

received June 30, 2014; received in revised form August 27, 2014; accepted September 25, 2014

Abstract

Functional ceramic nanopowders are prepared by means of CO_2 laser vaporization (LAVA) starting from coarse ceramic powders. The vaporization proceeds in a continuously flowing process gas at normal pressure. The nanoparticles (NP) are formed as a result of rapid gas phase condensation. Selected LAVA nanopowders are presented as promising candidates for future applications, e.g. drug targeting and magnetic resonance imaging, load-bearing ceramic implants, and biological fluorescence labeling, respectively. Starting from a hematite raw powder, ferrimagnetic Fe_2O_3 nanopowders are prepared. It is found that in an oxygen-free process gas maghemite (γ-Fe_2O_3) NP are formed. Applying oxygen as process gas leads to the formation of γ-and ε-Fe_2O_3 NP. Superparamagnetic composite NP are prepared from mixtures of hematite raw powder and quartz sand (SiO_2). NP comprising an intraparticular dispersion of alumina and tetragonal zirconia (t-ZrO_2) are obtained by means of the vaporization of a powder mixture of corundum (α-Al_2O_3) as the main component and t-ZrO_2. Europium-doped strontium aluminate ($SrAl_2O_4$) NP are prepared from a mixture of strontia (SrO), corundum, and Eu_2O_3. The as-prepared amorphous NP reveal a red photoluminescence emission under excitation with ultraviolet radiation. Annealing in a reductive atmosphere yields a crystalline Eu^{2+}:$SrAl_2O_4$ nanopowder that shows an intense green emission.

Keywords: Laser vaporization, ceramic nanoparticles, photoluminescence, Al_2O_3-ZrO_2, magnetic nanoparticles

I. Introduction

The unique physico-chemical properties of ceramic particles on the nanoscale are determined by their phase composition, size and size distribution, shape and specific surface area, as well as their morphological sub-structure. Nanoparticle (NP) processing technologies should allow the synthesis of a wide spectrum of compositions as well as the adaption of their properties to targeted applications. Numerous strategies were developed to synthesize functional ceramic NP including gas phase syntheses (e.g. chemical vapor synthesis, flame spray pyrolysis, thermal plasma synthesis, and laser pyrolysis), liquid phase syntheses (e.g. co-precipitation, sol-gel processing, hydrothermal synthesis, sonochemical synthesis), and solid state reactions (e.g. the mixed oxide technology) [1]. Gas phase and liquid phase syntheses, however, require specifically designed precursors to yield the desired materials, and solid state reactions are less suitable for the preparation of NP. Alternatively, gas phase syntheses using solid raw materials (e.g. inert gas condensation, spark discharge generation, laser ablation) can be applied to synthesize a wide range of ceramic nanopowder compositions.

In particular, the CO_2 laser vaporization (LAVA) has proved to be a suitable and flexible preparation process for ceramic nanopowders [2]. LAVA facilitates the continuous production of ceramic NP by means of rapid gas-phase condensation. Coarse ceramic powders with the same chemical composition as that of the desired NP are used as starting materials. Organic solvents requiring a drying process are not involved. Thus, contaminations of the NP by reaction by-products or residual solvents are excluded. The spectrum of nanopowders accessible with the basic LAVA process is considerably widened by the laser co-vaporization and subsequent co-condensation of multiple ceramic components. CoLAVA raw materials are homogeneous mixtures of at least two coarse ceramic powders. Composition and morphological sub-structure of the NP depend on the raw components and their mixing ratio, their reactivity as well as on their thermal behavior. Laser co-vaporization (CoLAVA) of different ceramic powders applied as a mixture facilitates the preparation of ceramic NP with different phase compositions and morphological sub-structures in a one-step process. LAVA- and CoLAVA-prepared NP include: i) single-phase ceramic NP, ii) nanocrystallites embedded in a glass matrix, iii) intraparticular dispersions, and iv) undoped and doped solid solutions. Here, we present the synthesis of several functional ceramic NP falling into these categories in order to exemplify the versatility of the CO_2 laser vaporization technique. The investigated compositions with inherent functionalities targeted to specific fields of applications include magnetic Fe_2O_3 and Fe_2O_3/SiO_2 composites, Al_2O_3/ZrO_2 dispersion ceramics, and photoactive Eu-doped $SrAl_2O_4$ solid solutions.

II. The (Co)LAVA technique

The LAVA process [2] starts from commercially available coarse ceramic powders (mean grain sizes: 1 µm – 1 mm). A

* Corresponding author: frank.mueller@uni-jena.de

CO_2 laser beam (wavelength: 10.59 µm, maximum power in continuous mode: 2 kW, peak power in pulsed mode: 3.5 kW) is focused (focus radius: 0.6 mm) onto the surface of the starting material (Fig. 1), which absorbs the high-intensity radiation (maximum intensities: 175 kW cm^{-2} in continuous mode, 310 kW cm^{-2} in pulsed mode). Utilizing a continuously flowing process gas, the raw powder heats up at normal pressure, vaporizes and forms a plasma. Expanding into the process gas, the plasma components recombine to neutral 'monomers'. Within the resulting supersaturated vapor, clusters emerge by means of homogeneous nucleation. The clusters act as nuclei for the condensation of melt droplets. The droplets grow as a result of surface condensation and coagulation. Finally, size and shape of the primary particles are set by solidification and crystallization. Driven by the process gas flow, the components of the interaction zone run through a steep temperature gradient. Owing to the rapid quenching, the lifetime of monomers and droplets is very limited and impedes their growth. Therefore, only nanoscale primary particles arise in a narrow size distribution. Directed by the process gas flow, the resulting NP aerosol is transported onto a candle filter. From here the nanopowder is finally extracted. Depending on the material and the process conditions, the laboratory LAVA setup yields nanopowders of several 10 g h^{-1} in a stable and continuous process. The mean particle size is controlled by the process gas flow rate through the condensation zone and by the laser regime. Higher flow rates and shorter laser pulses reduce the NP's mean size. Furthermore, the gas flow reduces the volume concentration of melt droplets and hot particles. Consequently, the probability of collision is significantly reduced and hard agglomeration by edge melting or sintering of the NP is suppressed.

III. Experimental

Here, continuous (power: 2 kW) or pulsed laser radiation (pulse frequency: 200 Hz, pulse length: 1 ms, peak power: 3.5 kW, mean power: 720 W) was used to prepare the presented nanopowders. A total process gas flow rate $\dot{v}_{tot}$ of 14.5 $m^3\ h^{-1}$ was applied. $\dot{v}_{tot}$ comprises the background gas flows $\dot{v}_{b1}$ = 4 $m^3\ h^{-1}$ and $\dot{v}_{b2}$ = 8.5 $m^3\ h^{-1}$ as well as the additional gas flow $\dot{v}_{add}$ = 2 $m^3\ h^{-1}$ which is directly fed through the zone of vaporization.

Standard characterization of the prepared NP. Transmission electron microscopy (TEM; JEM-3010 with EDX line scanning module, JEOL Ltd., Japan) was used to study the NP's morphology. Crystal properties and phase composition of the NP were investigated with X-ray powder diffraction (XRD; D8 Discover with GADDS, Bruker AXS GmbH, Germany) in combination with Rietveld refinement (Topas 4.2 software, Bruker AXS) applying structural models from the Inorganic Crystal Structure Database (ICSD).

Magnetic iron(III) oxide (Fe_2O_3) and iron(III) oxide-silica (Fe_2O_3-SiO_2) composite NP. Pure Fe_2O_3 NP were prepared from a hematite (α-Fe_2O_3) raw powder. The raw powder was vaporized applying continuous CO_2 laser radiation. In order to study the impact of the oxygen partial pressure within the condensation atmosphere on the crystallinity of the iron oxide NP, samples were prepared using Ar (0 vol% O_2), air (21 vol% O_2), and O_2 (100 vol% O_2), respectively, as condensation gases ($\dot{v}_{b1}$ and $\dot{v}_{add}$). Furthermore, iron oxide-silica composite NP were prepared from raw powder mixtures of α-Fe_2O_3 and SiO_2 (quartz sand). The raw powder mixtures were vaporized applying pulsed laser radiation and argon as condensation gas ($\dot{v}_{add}$). To study the formation of different morphologies of the composite NP depending on the α-Fe_2O_3-to-SiO_2 ratio in the raw powder mixture, samples were prepared from mixtures containing 33 wt% to 80 wt% of α-Fe_2O_3. The magnetic properties of the Fe_2O_3-based nanopowders were measured using vibrating sample magnetometry.

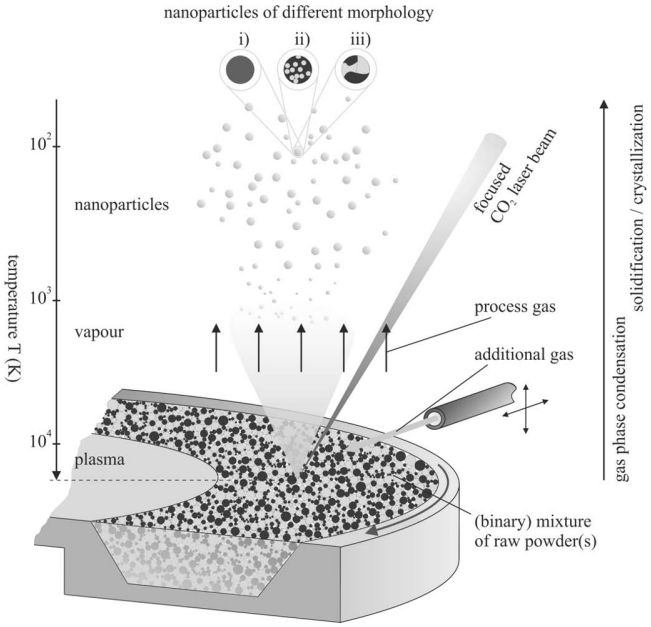

Fig. 1: Schematic of the (Co)LAVA principle and representation of the different process gas flows $\dot{v}_i$.

Al_2O_3-ZrO_2 dispersion NP. 74 wt% of corundum (α-Al_2O_3) and 26 wt% of tetragonal zirconia (t-ZrO_2, stabilized with 3 mol% of Y_2O_3) raw powders were homogeneously mixed. This mixture was vaporized applying pulsed CO_2 laser radiation and air as the process gas. EDX (energy-dispersive X-ray spectroscopy) line scans over single NP were conducted, in order to investigate the element distribution within the obtained NP.

Europium-doped solid solution strontium aluminate (Eu:$SrAl_2O_4$) NP. According to the reaction

$$SrO + Al_2O_3 \rightarrow SrAl_2O_4 \quad (1)$$

equimolar amounts of coarse strontia (SrO) and corundum (α-Al_2O_3) powders were homogeneously mixed. A portion of 5 wt% europium(III) oxide (Eu_2O_3) as dopant was added to one part of the powder mixture. Both starting mixtures were vaporized in air applying pulsed CO_2 laser radiation. The obtained nanopowder from the SrO/α-Al_2O_3 mixture with Eu_2O_3 was thermally treated (for 3 h up to temperatures of 1100 °C) in a reductive atmosphere (95 vol% nitrogen, 5 vol% hydrogen). Photoluminescence spectra (Tidas MMS/16 photometer equipped with a xenon lamp, J&M Analytik AG, Germany) of both nanopowder samples were measured at room temperature. The spectra were recorded in the emission wavelength λ_{em} range from 475 nm to 725 nm and at excitation wavelengths λ_{ex} between 300 nm and 400 nm.

IV. Results and Discussion

Magnetic Fe_2O_3 and Fe_2O_3-SiO_2 NP. NP based on iron oxide (Fe_xO_y) exhibit beneficial magnetic features such as crystallite-size-dependent ferrimagnetism or superparamagnetism, crystal-phase-dependent coercivity, or low Curie temperatures [3,4]. Ultra-small size and magnetic properties facilitate applications, e.g. as magnetic fluids, in data storage devices, or as magnetic filter material. In combination with their biocompatibility, the high specific loss power and the capability of being metabolized makes Fe_xO_y-based NP promising candidates for biomedical applications such as magnetic resonance imaging, drug delivery, or cancer treatment [5].

Various iron-oxide-based magnetic NP with specific compositional, morphologic, magnetic, and surface properties were successfully prepared. Starting from hematite, ferrimagnetic Fe_2O_3 NP (mean diameter: 22.4 nm) were obtained (Fig. 2a). In a nearly anoxic condensation atmosphere (argon) maghemite (γ-Fe_2O_3) formed as the main phase of the nanopowder. This powder is characterized by a high saturation magnetization (M_S = 72.2 Am^2 kg^{-1}). Its coercive field is H_C = 11.3 kA m^{-1}. Increasing the oxygen content of the condensation atmosphere resulted in the increasing formation of the ε-Fe_2O_3 polymorph as additional phase [6,7]. Simultaneously the saturation magnetization of the nanopowders decreases while their coercive field increases. This is due to the growing ε-Fe_2O_3 fraction. The ε-Fe_2O_3 polymorph has a comparatively small saturation magnetization ranging from 15 Am^2 kg^{-1} to 23 Am^2 kg^{-1} that depends on its size and morphology and a giant coercive field of H_C = 1.6 MA m^{-1} [8]. Using pure oxygen as condensation gas finally yielded an iron oxide nanopowder that contains 57 wt% γ-Fe_2O_3 and 43 wt% ε-Fe_2O_3. This nanopowder's saturation magnetization and coercive field are M_S = 37.8 Am^2 kg^{-1} and H_C = 16.6 kA m^{-1}, respectively.

The co-vaporization of α-Fe_2O_3 and SiO_2 yielded superparamagnetic composite NP comprising γ-Fe_2O_3 and amorphous silica (am-SiO_2). The intraparticle distribution of these phases and thus the NP's morphology depends on the mixing ratio of the raw powders. A raw powder mixture containing a small proportion of α-Fe_2O_3 (33 wt%) yielded Fe_2O_3 nanocrystallites (mean size: 6.5 nm) embedded in a spherical nanoscale glass matrix of am-SiO_2 (Fe_2O_3@SiO_2 NP, mean diameter: 30.3 nm, Fig. 2b). A high proportion of α-Fe_2O_3 (80 wt%) in the raw mixture yielded nanoscale *Janus* particles (Fe_2O_3|SiO_2 NP, mean diameter: 26.5 nm, Fig. 2c) composed of one polycrystalline superparamagnetic Fe_2O_3 hemisphere and one hemisphere of am-SiO_2. Both, the am-SiO_2 matrix and the am-SiO_2 hemisphere of the *Janus* particles represent reactive interfaces that are highly suitable for the chemical bonding of functionalizing ligands via silanization [9,10].

Al_2O_3-ZrO_2 dispersion NP. In ceramic process technologies the utilization of NP with their high specific surface area allows reduced sintering temperatures owing to increased sintering activity. NP also facilitate reduced grain sizes and in consequence a significant increase of the ceramics' strength. Dispersion ceramics consisting of Al_2O_3 (alumina) and ZrO_2 (zirconia) combine the high strength of alumina and high fracture toughness of zirconia [11]. This reinforcing effect can be increased by using NP comprising an intraparticle dispersion of both phases [12]. Thus, NP of an Al_2O_3-ZrO_2 dispersion were synthesized as potential starting material for the development of new load-bearing ceramics for, e.g. total joint prostheses [13]. Alumina-toughened-zirconia (ATZ) dispersion ceramic NP had already been successfully produced with the CoLAVA method starting from a raw powder mixture of mainly ZrO_2 with Al_2O_3 [2]. Here, the formation of zirconia-toughened-alumina (ZTA) NP by laser co-vaporization of tetragonal ZrO_2 (t-ZrO_2) and α-Al_2O_3 in inverse mixing ratio was investigated. The LAVA process yielded spherical, merely softly agglomerated NP (Fig. 3a) with a mean diameter of about 30 nm. High-resolution TEM micrographs show areas with differently oriented lattice fringes within a single ZTA NP, indicating its polycrystalline nature (Fig. 3b). The XRD analysis of the obtained nanopowder reveals the presence of transition alumina phases (cubic γ-, η-, and orthorhombic ι-Al_2O_3) as main fraction and tetragonal ZrO_2 as minor phase (Fig. 4). EDX line scans through the centers and the peripheral zones of exemplary NP suggest a radially varying distribution of the ZrO_2 and Al_2O_3 phases. The surface layer of the particles consists of Al_2O_3 while in the inner parts Al_2O_3 and ZrO_2 coexist.

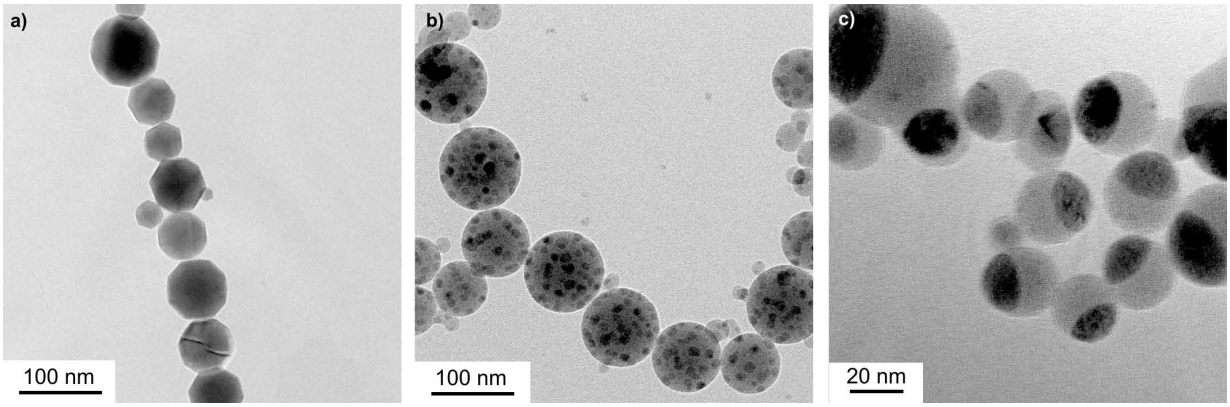

Fig. 2: TEM micrographs of iron-oxide-based magnetic NP prepared by means of (Co)LAVA: a) pure ferrimagnetic Fe_2O_3 NP, b) superparamagnetic Fe_2O_3@SiO_2 composite NP, and c) superparamagnetic Fe_2O_3|SiO_2 *Janus* NP.

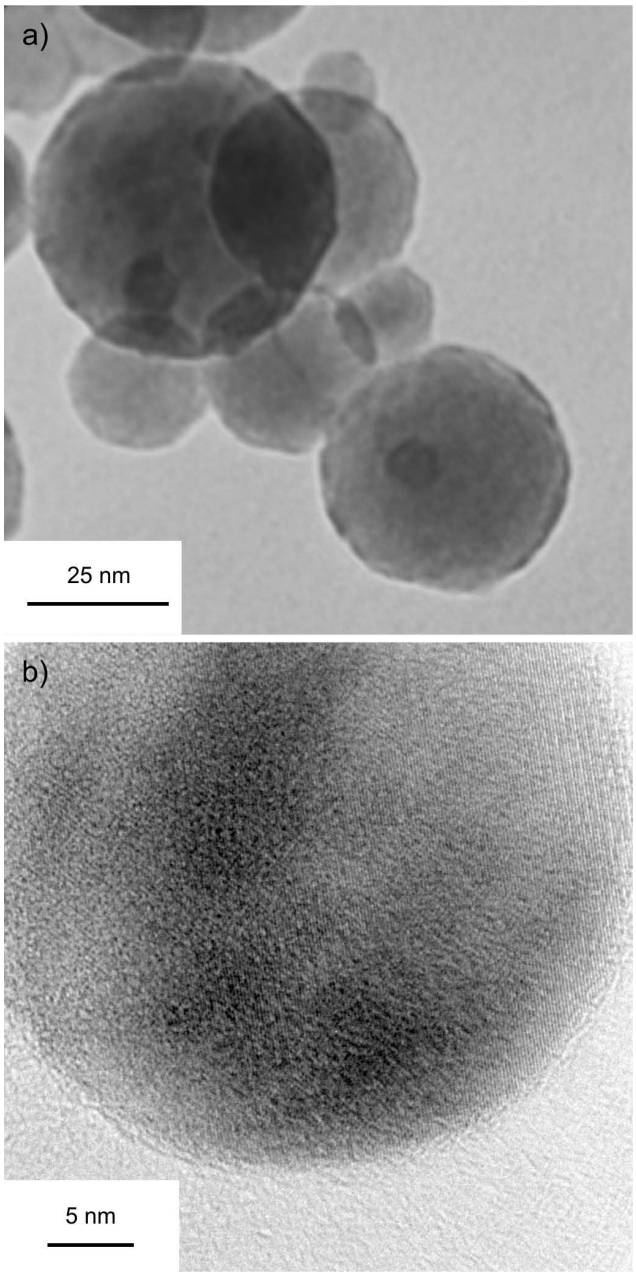

Fig. 3: a) TEM micrograph and b) high-resolution TEM micrograph of Al_2O_3-ZrO_2 (ZTA) NP prepared by means of CoLAVA.

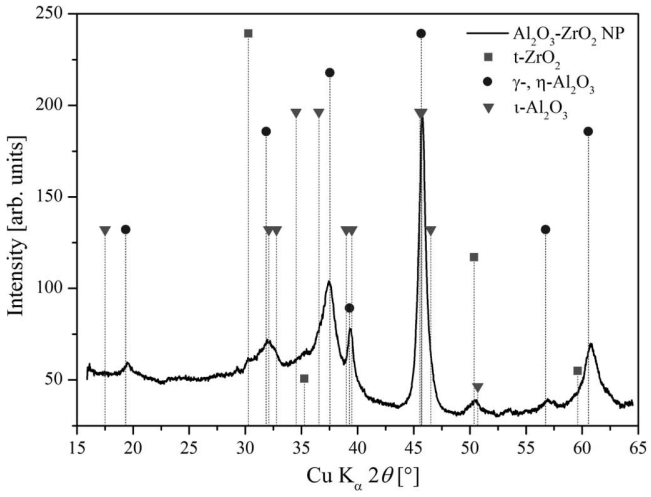

Fig. 4: XRD diagram of the LAVA-prepared Al_2O_3-ZrO_2 (ZTA) nanopowder.

ZrO_2 and Al_2O_3 exist in separate phases during the vapor condensation and subsequent crystallization in the CoLAVA process. ZrO_2 has a significantly higher evaporation temperature (b.p. 4300 °C) than Al_2O_3 (b.p. 2980 °C). Therefore, ZrO_2 condenses at first. The formed ZrO_2 droplets act as condensation nuclei initially for further ZrO_2 and below 2980 °C also for Al_2O_3 (Fig. 5). Within this temperature range both components mix owing to thermal flows within the melt droplets. Upon cooling below its melting temperature, ZrO_2 (m.p. 2680 °C) begins to crystallize. At the same time, the still liquid Al_2O_3 phase accumulates on the surface of the emerging ZrO_2 crystallites. From here, there are two possibilities for the further course of NP formation. Firstly, starting from one condensation nucleus a particle can grow by further addition of condensing Al_2O_3 (Fig. 5: model A). This would result in NP comprising a single zirconia core in an alumina shell. Secondly, several condensation nuclei collide and join forming a single particle (Fig. 5: model B). Cooling below a temperature of 2050 °C, Al_2O_3 starts crystallizing at the interface to the ZrO_2 nuclei. Now, there are again two ways crystallization can proceed: It simultaneously starts at many of the included ZrO_2 nuclei and proceeds until the whole particle is crystallized (Fig. 5: model B1). It is also conceivable that the crystallization emanates from one or only a few of the ZrO_2 nuclei (Fig. 5: model B2). In this case, the remaining liquid Al_2O_3 with embedded ZrO_2 crystallites is displaced by the crystallizing phase into the outer region of the particle. Both models B1 and B2 finally result in polycrystalline NP. But model B2 is favored by the intraparticle distribution of Al and Zr determined by the EDX line scans.

Eu-doped solid solution $SrAl_2O_4$ NP. Nanophosphors are of increasing importance for applications as markers in biological and medical imaging. Doped with lanthanide ions, ceramic NP provide a promising alternative to organic dyes for fluorescence biolabeling. Thus, photoluminescent *strontium aluminate NP-doped with europium ions* (Eu:$SrAl_2O_4$ NP) [14–18] were prepared as a representative of doped solid solution NP.

The co-vaporized educts SrO and α-Al_2O_3 react during their gas phase condensation forming amorphous spherical NP with diameters ranging from 10 nm to 80 nm (Fig. 6a). This is independent of the presence of the Eu_2O_3 dopant. Without dopant, the as-prepared nanopowders revealed no distinct photoluminescence maximum (Fig. 7). The nanopowder as-prepared from the powder mixture containing Eu_2O_3 exhibits a red emission at λ_{em} = 625 nm (Fig. 7) corresponding to a photon energy of E_{phot} = 1.98 eV. This is due to the Eu^{3+} ions [15] incorporated in the glass matrix. This emission reaches its maximum at an excitation wavelength of λ_{ex} = 394 nm (E_{phot} = 3.15 eV).

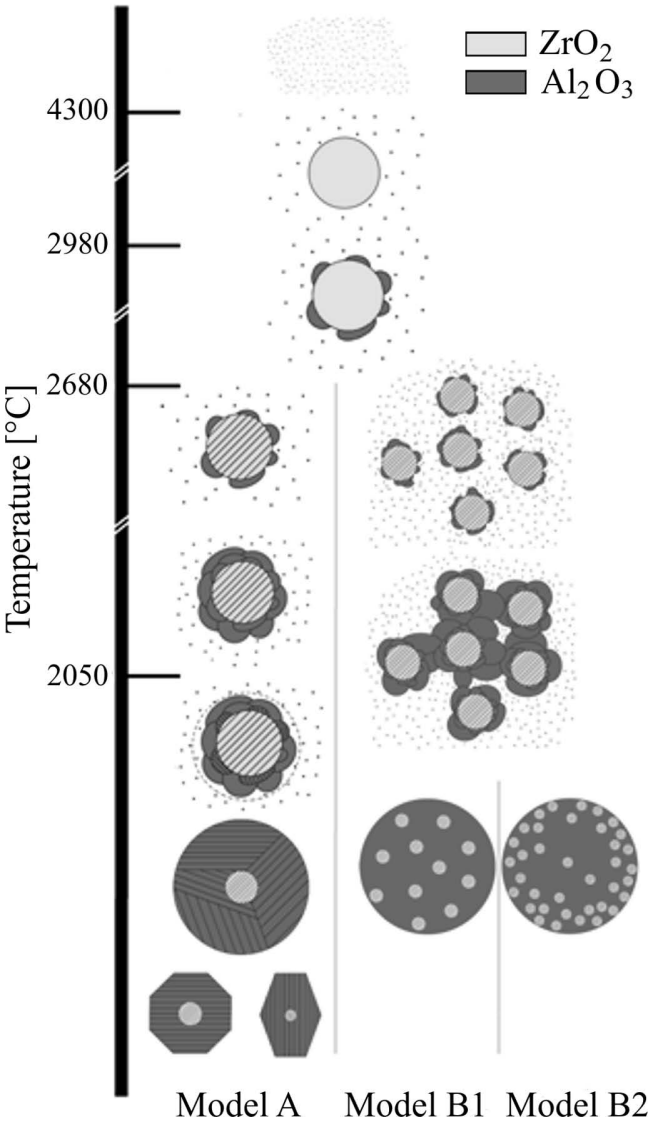

Fig. 5: Schematic representation of possible pathways for the formation of morphologic different Al_2O_3-ZrO_2 dispersion NP during the gas phase condensation.

Thermal treatment of the as-prepared doped nanopowder at reductive conditions and increasing temperatures results in an increasing formation of the $SrAl_2O_4$ spinel phase. At an annealing temperature of 1100 °C crystalline but slightly sintered NP were obtained (Fig. 6b). These particles contain more than 90 wt% of the $SrAl_2O_4$ spinel with minor proportions of $Sr_3Al_2O_6$ and $SrCO_3$. The presence of $SrCO_3$ is due to the usage of air as the CoLAVA process gas. This nanopowder reveals a strong green emission (Fig. 7) centered at λ_{em} = 525 nm (E_{phot} = 2.36 eV) with its intensity maximum at λ_{ex} = 364 nm (E_{phot} = 3.40 eV). This emission originates from Eu^{2+} ions incorporated into the crystal lattice of $SrAl_2O_4$ [17]. The red emission resulting from Eu^{3+} ions is no longer observable. This suggests that at the applied annealing conditions all Eu^{3+} from the Eu_2O_3 dopant has been reduced to Eu^{2+} [18].

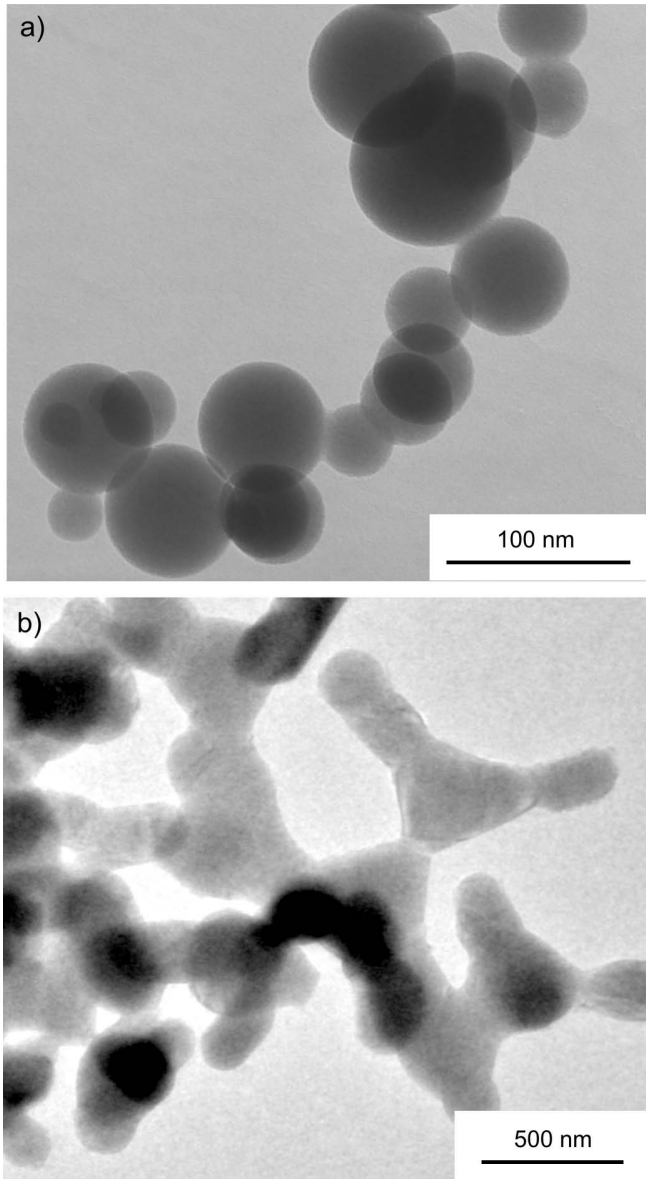

Fig. 6: TEM micrographs of the europium-doped nanopowders: a) as-prepared and b) after thermal treatment at 1100 °C and reductive conditions.

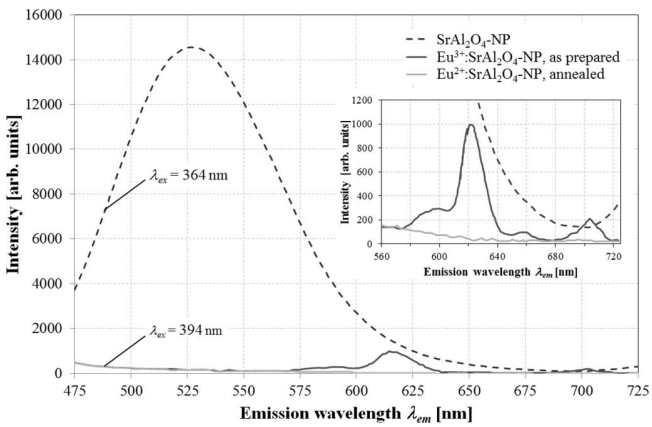

Fig. 7: Photoluminescence emission spectra of the as-prepared $SrAl_2O_4$ nanopowder without europium as well as of the europium-doped nanopowders as-prepared and after annealing at 1100 °C and reductive conditions.

V. Conclusions

CO_2 laser vaporization provides an excellent alternative for the preparation of functional ceramic nanopowders. Starting materials are widely available coarse ceramic raw powders. The obtained NP are chemically pure, merely softly agglomerated, and have a monomodal narrow size distribution. Depending on their composition they are spherically shaped or faceted. If mixtures of ceramic powders are applied as starting materials NP with different phase compositions and morphologies are accessible from a one-step process:

i) nanocrystallites embedded in a nanoscale glass matrix (e.g. γ-Fe_2O_3-SiO_2),
ii) NP comprising an intra-particle dispersion of phases (e.g. Al_2O_3-ZrO_2), and
iii) pure (e.g. $SrAl_2O_4$) or doped solid solution NP (e.g. Eu^{2+}:$SrAl_2O_4$).

This allows the design of novel functional composite NP for applications in e.g. optics, electronics, biomedicine, and catalysis as well as for technical ceramics with outstanding mechanical properties.

Acknowledgements

This work was supported by the Deutsche Forschungsgemeinschaft (DFG) under grant number MU1803/8 – 2 and by the European Research Council under the European Union's Seventh Framework Programs (FP/2007 – 2013)/ERC Grant Agreement n. 310637 (SMILEY). We acknowledge Dr Silvio Dutz, Institute of Photonic Technology, Jena, for the magnetic measurements of the Fe_2O_3-based NP and Professor Dr Cordt Zollfrank, Technische Universität München, and Dr Miroslaw Batentschuk, Friedrich-Alexander-University of Erlangen-Nuremberg, for the thermal treatment and the photoluminescence measurements of the Eu:$SrAl_2O_4$ NP.

References

1 Masala, O., Seshadri, R.: Synthesis routes for large volumes of nanoparticles, *Annu. Rev. Mater. Res.*, **34**, 41 – 81, (2004).

2 Kurland, H.-D., Grabow, J., Müller, F.A.: Preparation of ceramic nanospheres by CO_2 laser vaporization (LAVA), *J. Eur. Ceram. Soc.*, **31**, 2559 – 2568, (2011).

3 Cornell, R.M., Schwertmann, U.: The Iron Oxides: structure, properties, reactions, occurences and uses. 2nd edition, Wiley-VCH, Weinheim, Germany, 2003.

4 Hergt, R., Dutz, S., Röder, M.: Effects of size distribution on hysteresis losses of magnetic nanoparticles for hyperthermia, *J. Phys.: Condens. Matter*, **20**, 385214 – 385215, (2008).

5 Gupta, A.K., Gupta, M.: Synthesis and surface engineering of iron oxide nanoparticles for biomedical applications, *Biomaterials*, **26**, 3995 – 4021, (2005).

6 Tronc, E., Chaneac, C., Jolivet, J.P.: Structural and magnetic characterisation of ε-Fe_2O_3, *J. Solid State Chem.*, **139**, 93 – 104, (1998).

7 Stötzel, C., Kurland, H.-D., Grabow, J., Dutz, S., Müller, E., Sierka, M., Müller, F.A.: Control of the crystal phase composition of Fe_xO_y nanopowders prepared by CO_2 laser vaporization, *Cryst. Growth Des.*, **13**, 4868 – 4876, (2013).

8 Jin, J., Ohkoshi, S., Hashimoto, K.: Giant coercive field of Nanometer-sized iron oxide, *Adv. Mater.*, **16**, 48 – 51, (2004).

9 Tran, P.H.L., Tran, T.T.D., Vo, T.V., Lee, B.: Promising iron Oxide-based magnetic nanoparticles in biomedical engineering, *Arch. Pharmacal Res.*, **35**, 2045 – 2061, (2012).

10 Mout, R., Moyano, D.F., Rana, S., Rotello, V.M.: Surface functionalization of nanoparticles for nanomedicine, *Chem. Soc. Rev.*, **41**, 2539 – 2544, (2012).

11 Heimke, G., Leyen, S., Willmann, G.: Knee arthoplasty: recently developed ceramics offer new solutions, *Biomaterials*, **23**, 1539 – 1551, (2002).

12 Nikolay, D., Kollenberg, W., Deller, K., Oswald, M., Tontrup, C.: Manufacturing and properties of ZTA-ceramics with nanoscaled ZrO_2, *Ceram. Forum Int.*, **83**, 35 – 37, (2006).

13 Uribe, J., Geringer, J., Gremillard, L., Reynard, B.: Degradation of alumina and zirconia toughened alumina (ZTA) hip prostheses tested under microseparation conditions in a shock device, *Tribol. Int.*, **63**, 151 – 157, (2013).

14 Han, S.-D., Singh, K.C., Cho, T.-Y., Lee, H.-S., Jakhar, D., Hulme, J.P., Han, C.-H., Kim, J.-D., Chun, I.-S., Gwak, J.: Preparation and characterization of long persistence strontium aluminate phosphor, *J. Luminescence*, **128**, 301 – 305, (2008).

15 Poort, S.H.M., Blokpoel, W.P., Blasse, G.: Luminescence of Eu^{2+} in barium and strontium aluminate and gallate, *Chem. Mater.*, **7**, 1547 – 1551, (1995).

16 Kostova, M.H., Zollfrank, C., Batentschuk, M., Goetz-Neunhoeffer, F., Winnacker, A., Greil, P.: Bioinspired design of $SrAl_2O_4$:Eu^{2+} phosphor, *Adv. Funct. Mater.*, **19**, 599 – 603, (2009).

17 Aroz, R., Lennikov, V., Cases, R., Sanjuan, M.L., de la Fuente, G.F., Munoz, E.: Laser synthesis and luminescence properties of $SrAl_2O_4$:Eu^{2+}, Dy^{3+} phosphors, *J. Eur. Ceram. Soc.*, **32**, 4363 – 4369, (2012).

18 Zollfrank, C., Gruber, S., Batentschuk, M., Osvet, A., Goetz-Neunhoeffer, F., Dittrich, S., Grabow, J., Kurland, H.-D., Müller, F.A.: Synthesis of Eu-doped $SrAl_2O_4$ nanophosphors by CO_2 laser vaporization, *Acta Mater.*, **61**, 7133 – 7141, (2013).